ADVANCED MATERIALS
www.advmat.de

Topological Interlocking and Geometric Stiffening as Complementary Strategies for Strong Plant Shells

Jessica C. Huss, Sebastian J. Antreich, Jakob Bachmayr, Nannan Xiao, Michaela Eder, Johannes Konnerth, and Notburga Gierlinger**

Many organisms encapsulate their embryos in hard, protective shells. While birds and reptiles largely rely on mineralized shells, plants often develop highly robust lignocellulosic shells. Despite the abundance of hard plant shells, particularly nutshells, it remains unclear which fundamental properties drive their mechanical stability. This multiscale analysis of six prominent (nut)shells (pine, pistachio, walnut, pecan, hazelnut, and macadamia) reveals geometric and structural strengthening mechanisms on the cellular and macroscopic length scales. The strongest tissues, found in walnut and pistachio, exploit the topological interlocking of 3D-puzzle cells and thereby outperform the fiber-reinforced structure of macadamia under tensile and compressive loading. On the macroscopic scale, strengthening occurs via an increased shell thickness, spherical shape, small size, and a lack of extended sutures. These functional interrelations suggest that simple geometric modifications are a powerful and resource-efficient strategy for plants to enhance the fracture resistance of entire shells and their tissues. Understanding the interplay between structure, geometry, and mechanics in hard plant shells provides new perspectives on the evolutionary diversification of hard seed coats, as well as insights for nutshell-based material applications.

Biological shells display a large morphological,[1,2] biochemical,[3] and mechanical diversity[4,5] across and within kingdoms. A common feature of all shells is their small thickness relative to the radius. In seed plants, hard shells typically occur in the process of fruit wall (pericarp) and seed coat (testa) formation, where they serve as protective covers for the delicate embryos.[6] During development on the parental plant, individual layers of the pericarp or the testa may harden substantially via extensive secondary cell wall formation and lignification.[7,8] Cracking these shells after they have reached maturity requires remarkably high compression forces in some species, ranging from 300 to ≈700 N for pecans, walnuts, and hazelnuts; and up to ≈4000 N for macadamia shells.[9] In the natural environment, the encapsulated seed, known as the dispersal unit or diaspore, is typically dispersed by granivorous and scatter-hoarding animals.[10] After dispersal and storage near the soil surface or underground, seed germination may start with the uptake of water.[11] Some diaspores endure exceptionally long storage periods: archaeologically recovered seeds of *Phoenix dactylifera* were successfully germinated after ca. 2000 years.[12] Despite their biological importance, we still know little about the structural and mechanical properties of hard plant shells. In macadamia shells, structural, and mechanical analyses relate their high fracture resistance mainly to a high tissue density and the distinct cellular arrangement.[9,13] However, the detailed contributions of shell geometry and tissue structure, including sutures and water gaps,[14–16] remain elusive in most species.

In this work, we identify the cellular and macroscopic features that strengthen plant shells substantially. Since many edible nuts (only some of the commonly named "nuts" are true botanical nuts) exhibit hard and strong shells, we compare the structural and mechanical properties of six commonly known (nut)shells: the testa of *Pinus koraiensis* and *Macadamia integrifolia*; and the woody pericarp layers of *Juglans regia*, *Pistacia vera*, *Corylus maxima*, and *Carya illinoiensis* (**Figure 1**a). Our experiments include mechanical testing, as well as histochemical staining and 3D imaging via X-ray microtomography and serial block face scanning electron microscopy.

Cross-sections of entire shells (Figure 1b) and tissues (Figure 1c) indicate a more heterogeneous structure in pecan, hazelnut, and macadamia shells in comparison to pine, pistachio, and walnut shells. The segmentation of cells in 3D shows that, surprisingly, the latter three shells consist of only one main cell type, respectively (Figure 1d). These are nearly

Dr. J. C. Huss, S. J. Antreich, J. Bachmayr, N. Xiao, Prof. N. Gierlinger
Institute of Biophysics
University of Natural Resources and Life Sciences Vienna
Vienna 1190, Austria
E-mail: jessica.huss@boku.ac.at; burgi.gierlinger@boku.ac.at
Dr. J. C. Huss, Dr. M. Eder
Department of Biomaterials
Max Planck Institute of Colloids and Interfaces
Potsdam-Golm 14476, Germany
Prof. J. Konnerth
Institute of Wood Technology and Renewable Materials
University of Natural Resources and Life Sciences Vienna
Tulln an der Donau 3430, Austria
The ORCID identification number(s) for the author(s) of this article can be found under https://doi.org/10.1002/adma.202004519.

DOI: 10.1002/adma.202004519

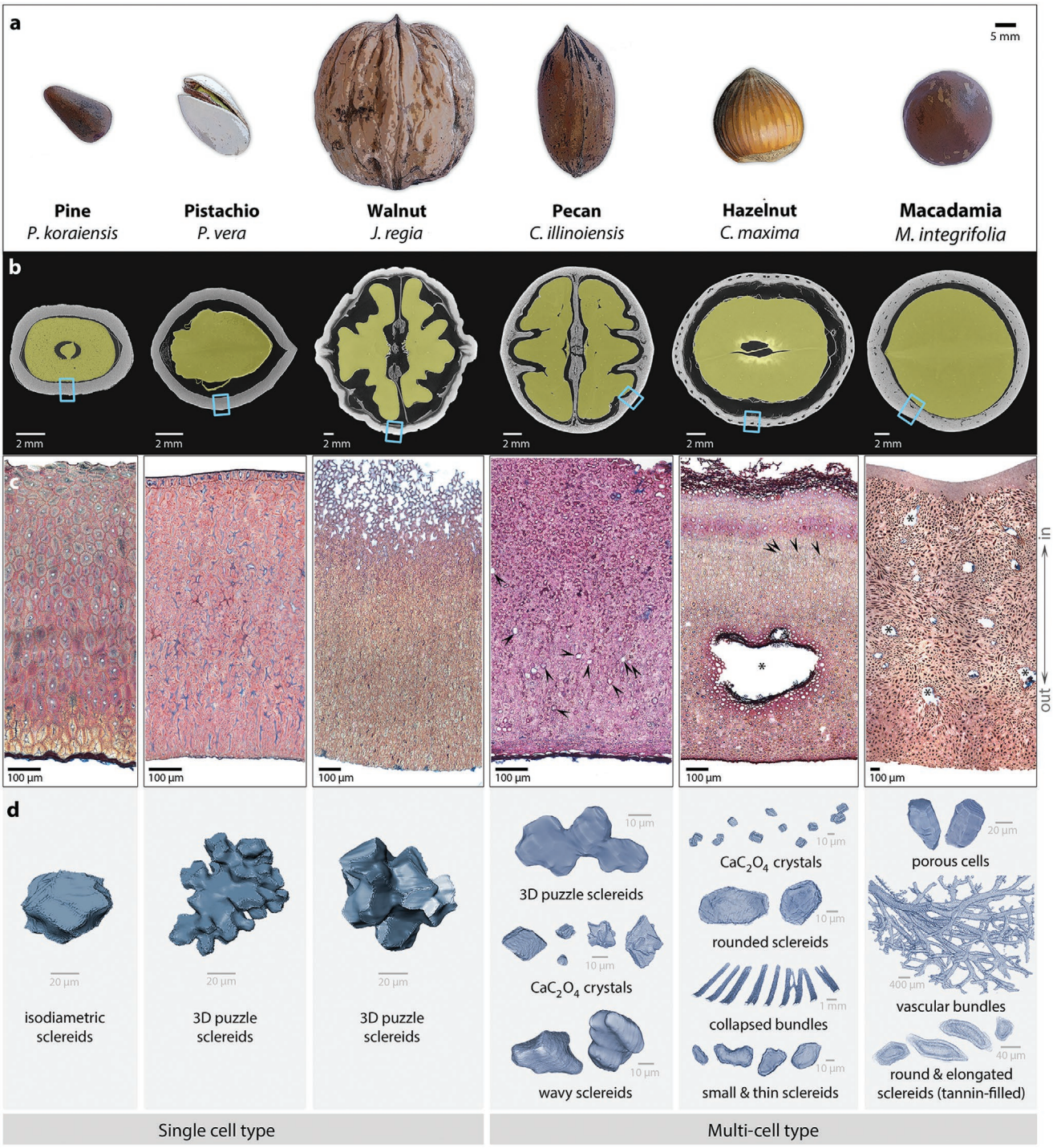

Figure 1. Overview and structural arrangement of (nut)shells on different hierarchical levels. a) Typical morphology of the six investigated shells. At maturity, some pistachios may split open naturally (shown here), whereas all other shells remain closed. b) Cross-sections of the six investigated diaspores based on X-ray micro-tomography show the overall shape, thickness, and size of shells and seeds (yellow). c) Light microscopy images of shell cross-sections stained with Fuchsin-Chrysoidin-Astrablue (FCA), revealing strong lignification (red/orange) in all tissues, except for the weakly lignified inner part of walnut shells (cellulosic tissue stains blue). Vascular bundles (*) appear as holes in macadamia as a result of cutting artefacts and consists of thin-walled, helical vascular bundles, which were easily pulled apart during tensile testing (Figure 2g). Calcium oxalate crystals in hazelnuts and pecans (arrows) remained unstained. Larger images are provided in Figure S2, Supporting Information. d) Main cell types and shell components in 3D based on X-ray nano-tomography and serial block face scanning electron microscopy; indicating two classes of shell organization.

isodiametric sclereids in pine, 3D-puzzle sclereids with numerous small lobes in pistachio, and big-lobed 3D-puzzle cells in walnut shells. Pecan, hazelnut, and macadamia shells, in contrast, include multiple cell types and components (Figure 1d): pecan shells consist of ≈40 µm small and weakly lobed 3D-puzzle sclereids in the inner shell part, followed by wavy sclereids in the outer part along with diverse calcium oxalate[17] crystals (Figure S1a, Supporting Information). In hazelnuts, elongated and round sclereids in variable sizes make up the majority of the shell. Collapsed vascular bundles and a thin layer of cubic calcium oxalate crystals (Figure 1c and Figure S1b, Supporting Information) are also incorporated. In macadamia shells, a layer of highly porous, polygonal cells lines the inside (Figure 1c) of one half (around the micropyle, where the radicle will emerge), followed by a highly branched network of thin-walled vascular bundles (Movies S1 and S2, Supporting Information) that are interspersed by round and elongated, tannin-filled sclereids and sclerenchymatous fibers (Figure 1d and Movie S2, Supporting Information). Based on the main cell types in each tissue, we can distinguish two classes of plant shells: 1) single cell type and 2) multi-cell type structures.

Mechanical testing reveals that the tissues of pistachio and walnut shells, both composed of 3D-puzzle cells, reached the highest ultimate tensile stress (UTS); with means at 68.9 ± 5.1 MPa and 64.5 ± 8.9 MPa, respectively, and maxima at ≈78 and ≈76 MPa (**Figure 2**a, Figure S3, Supporting Information). Despite having 3D-puzzle cells, pecan shells are weak; with a mean UTS of 33.8 ± 4.9 MPa. We link this to the smaller puzzle size and number of lobes in the inner part of the shell, and to the presence of almost non-lobed sclereids in the outer part of the shell (Figures 1d and 2e). These cell shapes interlock only weakly, as indicated by the predominant crack propagation along the interface between the cells (Figure 2e). As the only fiber-reinforced shell, macadamia specimens show a lower UTS (similar to ref.[13]) than pistachio and walnut shells, but a slightly higher tensile modulus and a similar compressive modulus (Figure S4, Supporting Information). Fracture predominantly occurs at the vascular bundles (Figure 2g), and includes cell wall fracturing and interfacial separation of fibers. In hazelnut and pine shells (Figure 2d,f), cells fracture predominantly near the interface (middle lamella or primary wall); whereas walnut and pistachio puzzles fracture through the cell walls (Figure 2h,i). The middle lamella forms the interfacial matrix between plant cells and is known to be prone for crack propagation due to its lower stiffness when compared to the cell walls.[18] We expect that this mode of crack propagation along the middle lamella also applies to our samples, and that it leads to immediate failure in shells with round cells (based on Figure 2d–f) due to their low ability to deflect or arrest a propagating crack. In large 3D-puzzle sclereids, however, crack propagation along the middle lamella does not result in global failure, because the cell walls are able to interlock (Figure 2h–i) until stress levels exceed the wall strength. This mechanism fits into the concept of topological interlocking in biological microstructures.[19,20] Despite their similar cell type and tensile strength, differences exist between walnut and pistachio: all walnut specimens consistently exhibit brittle failure (Figure 2b), while pistachios show a pronounced elongation phase before failure around 5–8% strain. Computational predictions and experiments with 3D printed blocks[21,22] show that strength and ductility increase with increasing waviness of the lobes and increasing level of interlocking. Similarly, we attribute the higher ductility in pistachio to the larger number of lobes per cell and a wavier shape of lobes that may fracture gradually at high tensile stresses (no pull-out, Figure 2i). Furthermore, cracks that propagate through cell walls are more likely to be arrested in the relatively large lumina of pistachio sclereids when compared to walnut sclereids in the outer shell part (Figure S2, Supporting Information). The high strength of interlocked puzzle cells manifests itself also during compressive loading, where walnut specimens reached a mean maximum stress of 222.7 ± 45.8 MPa, while macadamias only reached 125.6 ± 19.0 MPa (Figure 2c, Figure S4b, Supporting Information), despite their higher shell density (Table S1, Supporting Information). Interestingly, in both species, the compressive strength exceeds the respective tensile strength. This property provides functional advantages for seeds, because shells may be more difficult to crack from the outside, for example, by rodents and birds,[23] than from the inside by the expanding embryo during germination.[24]

Having a strong shell is only advantageous until the onset of germination—a process that involves water uptake and controlled fracture formation.[16,25] This is typically achieved by incorporated structural discontinuities (sutures), which are also well visible in walnut and macadamia shells: a long band of water permeable, non-lignified, thin-walled tissue encompasses the pericarp in walnuts (360°, **Figure 3**a), whereas the testa of macadamias only contain two small perforations with porous (micropyle, Figure 3b) and weak tissue (hilum); in addition to a comparatively short (<90°) V-shaped notch (Figure 3b–c). The vascular bundles enter the shell through the hilum and form a branched network within the shell (Figure 3c and Movie S1, Supporting Information). Along the minute 180° surface notch, the vascular network shows a 180° discontinuity, which lacks sclerenchymatic fibers. Based on these tissue arrangements, both regions appear to be predetermined breaking points for germination, and cause anisotropic fracture in entire shells.[13]

During equatorial compression (**Figure 4**a), with smaller effects of sutures, macadamias still clearly stand out with a remarkable mean fracture force of ≈2400 N.[9,13] As indicated by the mechanical data for the different tissue types (Figure 2), the difference of an order of magnitude in comparison to other entire shells (Table S1, Supporting Information) cannot arise from the tissue structure alone, but is instead caused by geometric advantages: if we accept that the thin shell requirement ($t/r \ll 1$; r: radius, t: thickness) is met for our shells (values from cross-sections range from 0.12 to 0.36), we can approximate the axial stiffness K in the loading direction by following the approach for symmetric ellipsoidal shells.[5,26] Generally, K scales proportionally to $Et^2\kappa$ in thin ellipsoidal shells; with shell thickness t, mean curvature κ at the loading point, and Young's modulus E. Based on the thin shell assumption, the axial stiffness has the largest value for macadamia shells in comparison to the other shells (Figure 4a). Due to the power-law relation, it is evident that the most effective way of increasing K is to increase t. For shells with $t \leq 1$ mm (Figure 4b), the effect of geometric stiffening is relatively small, irrespective of the shell shape and size. This might explain the similar range of fracture

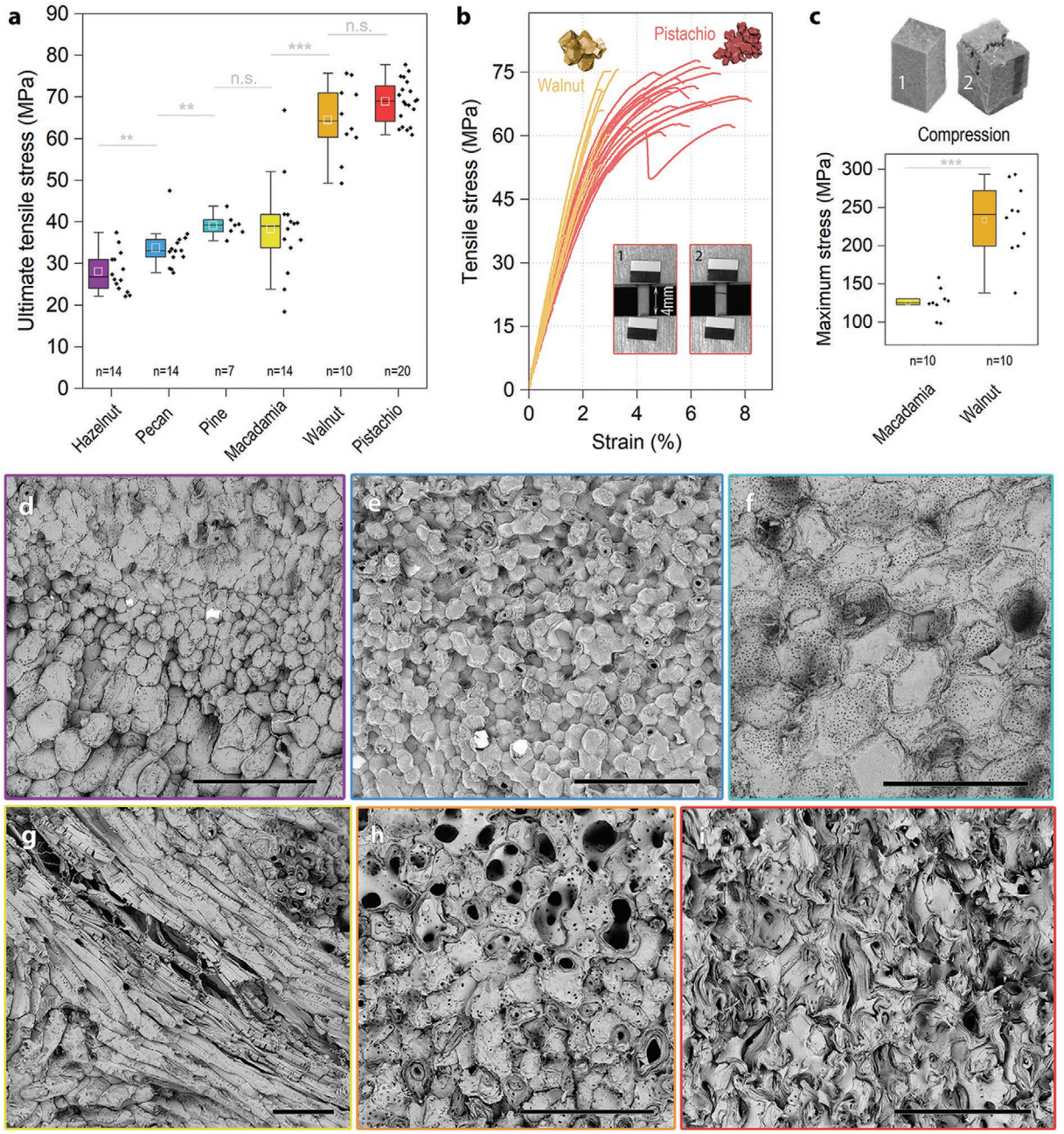

Figure 2. Mechanical properties of longitudinal specimens from six (nut)shells. a) Ultimate tensile stress (box: 25–75%, whisker: 1.5 IQR) for all tested specimens (Figure S3, Supporting Information). Shell moisture content ranged between 5 and 11% during testing. b) Stress–strain curves of the two strongest shell tissues (walnut and pistachio) with their 3D-puzzle cells and video images of a pistachio specimen during testing; showing initial state (1) and failure (2). c) Maximum stress of macadamia (exemplary samples shown) and walnut shell specimens with aspect ratios of 1:1:2 before (1) and after (2) quasi-static compression testing. d–i) Fracture surfaces after tensile testing (scale bars: 100 µm): d) tissue in the crystal region of hazelnut shells; e) transition zone in pecan shells, showing 3D-puzzle cells in the inner shell parts (top) and wavy sclereids in the outer parts (bottom); f) pine sclereids with many pits and delaminated primary walls; g) fractured vascular bundle with thin cell walls in macadamia; h) fractured cell walls of a walnut specimen in the inner (top) and outer part (bottom); i) strongly fractured cell walls of 3D-puzzle cells in pistachio shells.

forces for pecan, pine, and pistachio, but not necessarily for walnuts (Figure 4a). We speculate that the surface structure and large suture area in walnuts lead to excessive stress concentration during compression, resulting in early fracture. In macadamia shells, t (and E) is largest (Table S1, Supporting Information); showing that a weaker tissue (Figure 2) can still be highly functional when it is assembled into a geometrically advantageous shell (Figure 4b). Similarly, the effect of geometric stiffening is also well visible in hazelnuts.

In summary, we compared the microstructure and geometry of different animal-dispersed plant shells and discovered at least four major strategies that lead to strengthening on

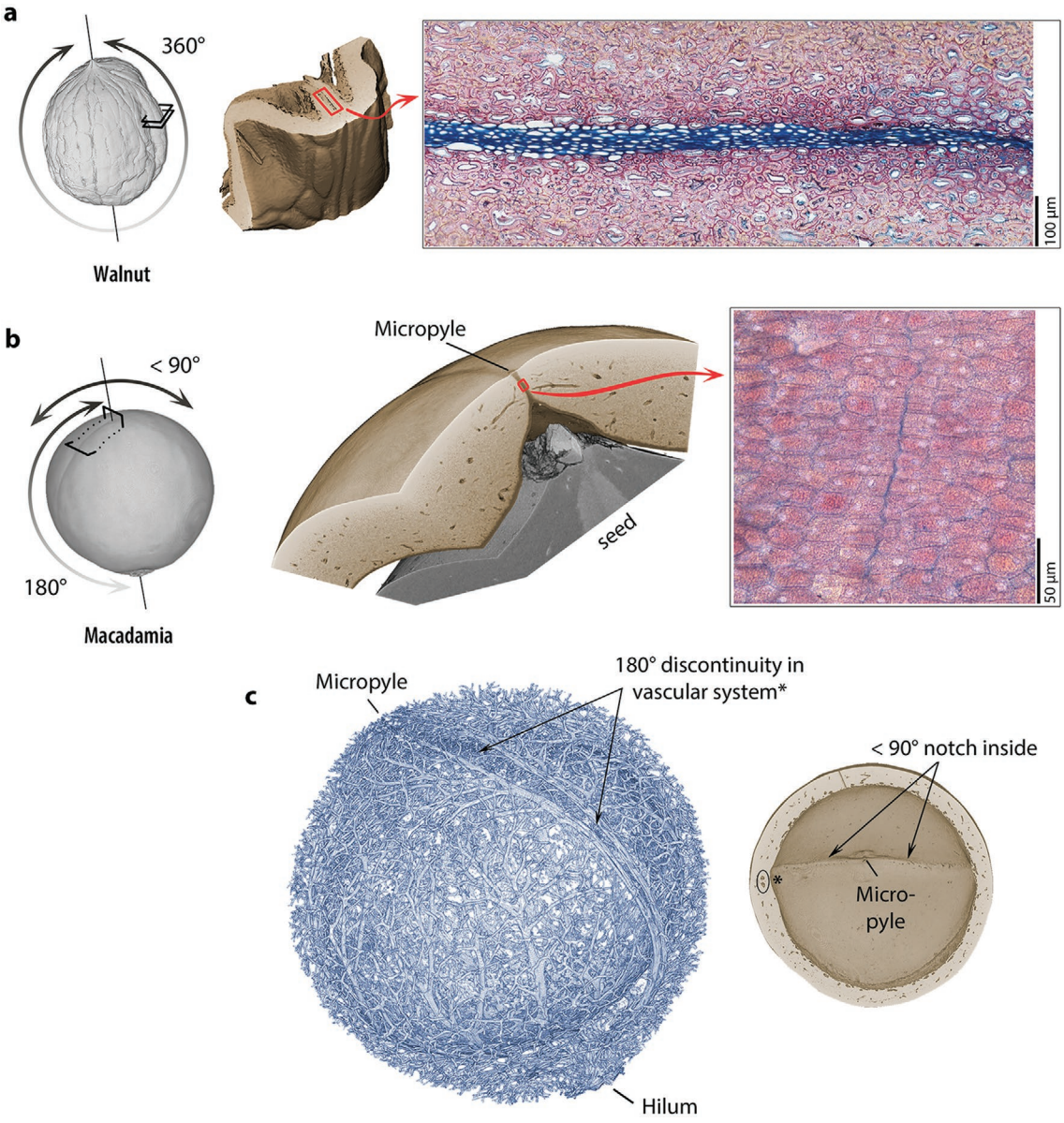

Figure 3. Length, position and structure of sutures in a) the pericarp of walnuts, and b) the testa of macadamias. 3D representations indicate the length (in degrees) of sutures and notches on whole shells, while fragments show the position of FCA stained sections (red: lignin; blue: cellulose). c) The segmented vascular network in macadamia shells shows a one-sided 180° discontinuity (Movie S1, Supporting Information), whose position is indicated (*) in the upper half of the shell, where it overlaps partly with the distinct notch and ends in the micropyle. Overview of all shells in Figure S5, Supporting Information.

two hierarchical levels: 1) on the tissue level, the development of large, thick-walled and strongly lobed 3D-puzzle cells adds significant tensile and compressive strength via topological interlocking, while, on the macroscopic level, 2) an overall increased shell thickness, 3) spherical shape and 4) small size increase the fracture resistance via geometric stiffening. From these insights, we conclude that plants are in principle able to increase the strength of their shells in a resource-efficient way by means of simple structural and geometrical adaptations. Seed plants may have exploited these principles during evolution, allowing them to increase seed size,[27,28] to enhance protection,[29] and to drive diversification.[30–32] Exploiting these principles may be useful for designing functional materials, such as resource-efficient packaging structures or seed coatings for conservational purposes.

Experimental Section

Origin of Nuts: Mature nuts of *P. koraiensis* were obtained in 2018 from Changbai (China). Mature specimens of *P. vera* were collected in Bronte, Sicily (Italy) on September 10th, 2019, and in Kerman (Iran) in September 2019. Young nuts from Kerman were harvested in June 2019. *J. regia* nuts (Cultivar Geisenheim 120) were grown in the Versuchszentrum Jedlersdorf (BOKU Vienna) and harvested at maturity on September 19th, 2018 and October 1st, 2019. Young nuts were collected in July 2018. *C. illinoiensis* fruits also originate from the Versuchszentrum

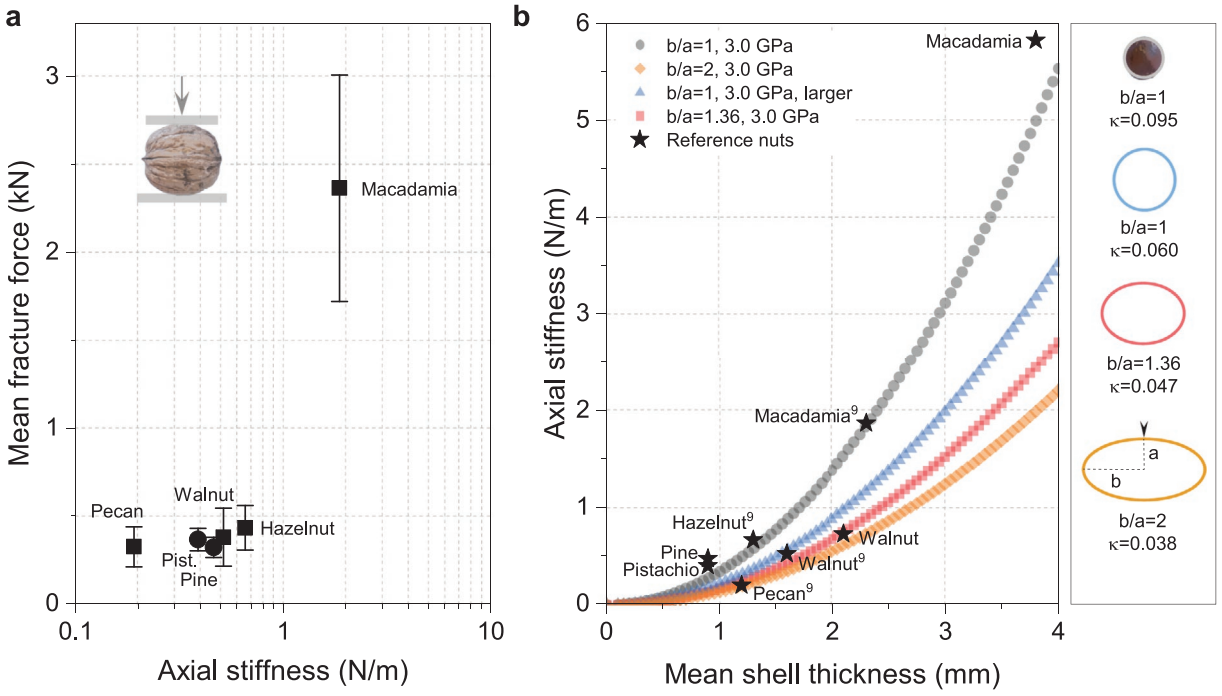

Figure 4. Mean fracture force and axial stiffness of entire shells during equatorial compression. a) Mean fracture force (± SD) in comparison to the axial stiffness of our own (circles, see also Table S1, Supporting Information) and reference shells[9] (squares). b) Axial stiffness as a function of shell thickness for two spheres and two prolate spheroids of variable shapes (b/a) and sizes ($a_{grey} = 10.5$ mm; $a_{blue} = a_{red} = a_{orange} = 16.5$ mm) with a constant Young's modulus ($E = 3.0$ GPa). Experimental values for E are given in Table S1, Supporting Information, for all shells. The stiffness increases with increasing shell thickness, increasing sphericity and decreasing size.

Jedlersdorf; harvested in October 2018 and October 14th, 2019. Young nuts were harvested on September 3rd, 2019. *C. maxima* was grown in Ordu, Karadeniz (Turkey) and mature nuts harvested in September 2019. *M. integrifolia* nuts were ordered online (unknown origin).

X-ray Tomography and 3D Visualization: Mature nuts were scanned in an EasyTom 150/160 system (RX solutions) with a Hamamatsu micro-focus tube set to a current of 250 µA and a voltage of 40 kV. Projections were collected with a flat panel detector, acquiring 1440 images with a frame rate of 2 s^{-1}, averaging 10 images. Small shell fragments of young (walnut, pecan, pistachio, for easier segmentation) and mature shells (all six species) were scanned at higher resolutions with the Hamamatsu nano-focus tube (LaB6 filament), set to a current of 150 µA and a voltage of 40 kV with projections collected every second, averaging between 8 and 10 images. Reconstruction was performed with XAct 2 (RX solutions), data segmented in Amira (version 6.1, FEI) and Drishti (version 2.6, Ajay Limaye, Australian National University). The voxel size of 0.4 µm (lower limit) was not sufficient for segmentation of pecan shells and the inner layer of macadamia and were obtained via serial-block face SEM.

Serial-Block Face SEM: Trimmed shell volumes of ≈1 mm^3 were immersed in fixation solution, containing 3% glutaraldehyde in 100×10^{-3} M sodium cacodylate (pH7.4), and stored at 4 °C overnight, then rinsed three times with 150×10^{-3} M cacodylate buffer and post fixed with 2% osmium tetroxide and 0.2% ruthenium red in 150×10^{-3} M cacodylate buffer for 1 h at room temperature (RT). After washing with cacodylate buffer, samples were incubated in freshly prepared thiocarbohydrazide solution (1% w/v in aqua dist.) for 45 min, followed by washing with aqua dist. and with a 2% osmium solution for 1 h. Samples were washed again with aqua dist. and immersed into 0.5% uranyl acetate and stored overnight at 4 °C. After more washing cycles with aqua dist., samples were transferred in Waltron's lead aspartate solution (30 min, 65 °C) and washed with aqua dist. Dehydration was performed in solutions of 30%, 50%, 70%, 90%, 100%, 100% ethanol in water, followed by 100%, 100% acetone (each step 30 min, RT) prior to infiltration with 25% low-viscosity resin in acetone and overnight storage (4 °C). Then samples were transferred into 50% and further into 75% resin (4 h each), until 100% resin overnight (4 °C) followed by a second round of 100% resin (6 h, RT) and polymerization in flat molds (65 °C, 48 h). Sample blocks were trimmed to 0.5 mm^3 with a glass knife on a UC-7 ultramicrotome (Leica), and glued onto a stub with silver cement, coated with a 10 nm gold layer in a sputter coater (Leica) and 100 $µm^2$ areas scanned in the Apreo-SEM (FEI) with a voltage of 1.18 kV, a current of 100 pA, and a dwell time of 3 µs. Approximately 1000 slices were cut with a slicing depth of 100 nm, controlled by the software Maps 3.4 VS (FEI). The image stacks were registered in ImageJ (version 1.52, W. Rasband, NIH) and then further processed in ImageJ, Amira (version 6.1, FEI) or Drishti (version 2.6, Ajay Limaye, Australian National University).

Histological Staining with FCA: 8 µm thick sections were cut with a rotary microtome RM 2255 (Leica) and immersed into drops of FCA for 2–3 h, followed by stepwise washing with aqua dist., 30% ethanol, 70% ethanol, and 100% isopropyl alcohol. The stained sections were embedded in Euparal (Roth) and imaged with a light microscope (Labophot-2, Nikon). The FCA solution consisted of 0.1 g Fuchsin, 0.143 g Chrysoidin, and 1.25 g Astrablue in 1000 mL aqua dist. and 20 mL acetic acid.

Tensile Tests: Longitudinal (mature) shell segments were trimmed to a length of ≈0.8–1 cm, width of ≈1.5–2 mm and thickness of ≈0.8–1.2 mm (no thickness trimming in *P. koraiensis*, *P. vera*, and *C. illinoiensis* due to thin shells) with a cryostat CM 3050 S (Leica) at –15 °C (Figure S3, Supporting Information). Both ends of the air-dried specimens were glued into holders (with a free length of 4 mm), consisting of three-layered model aircraft plywood from birch (1 mm thick, 45 mm long, and 18 mm wide) using superglue (Loctite 454, Henkel) for the sample and wood glue (Ponal Express, Henkel) for the three support parts on each end, following the same protocol of Antreich et al.[8] The construction was compressed with clothes pegs during drying for 30 min; further glue hardening occurred for another 3 days prior to testing. Loading

was performed with a test speed of 0.004 mm s^{-1} on a 2.5 kN materials testing machine (zwickiLine Z2.5, Zwick-Roell), in combination with a 1 kN load cell (Zwick-Roell) and a video extensometer (videoXtens, Zwick-Roell), measuring the length changes after preloading samples with 1N (initial clamp distance: 4.5 cm). Strains were calculated for the free sample length. Mature shells were tested of *P. koraiensis* ($n = 7$; data from Antreich et al.[8]); *P. vera* ($n = 10$ from Iran; $n = 10$ from Sicily); *J. regia* ($n = 10$ from the year 2019); *C. illinoiensis* ($n = 14$ from the year 2019); *C. maxima* ($n = 14$); *M. integrifolia* ($n = 14$). Imaging of fracture surfaces was performed with the Apreo-SEM; using a voltage of 1 kV and a current of 50 pA.

Compression Tests: Longitudinal shell segments were trimmed to cuboid specimens with a cryostat with most dimensions in the range of 2 × 2 × 4 mm; and a strict aspect ratio of 1:1:2. Samples (*M. integrifolia* $n = 10$; *J. regia* $n = 10$ from the year 2019; the other shells were too thin for testing) were air dried at ambient conditions (24 °C, 23% RH) for several days before testing (23 °C, 50% RH) on the system Z020 (Zwick-Roell). Samples were compressed with a speed of 0.5 mm min^{-1} and a pre-force of 5 N. A 500 N load cell was used for small specimens and a 20 kN load cell (both Zwick-Roell) was used for larger specimens and whole nuts (compression perpendicular to suture as depicted in Figure 4a).

Data Analysis: Ultimate tensile stress and maximum (compressive) stress represent the maximum values recorded for each specimen (Figure S4b, Supporting Information). Elastic moduli were determined at the initial phase of the stress strain curve, after sample alignment. For statistical analysis, the non-parametric Wilcoxon/Mann–Whitney test in OriginPro (version 8, OriginLab) is used with significance levels of $\alpha =$ 0.05*, 0.01**, 0.001***.

Supporting Information

Supporting Information is available from the Wiley Online Library or from the author.

Acknowledgements

The authors thank Martin Felhofer, Daniel Werner, Petra Leibner and Nils Horbelt for technical support, as well as Jaqueline Friedmann, Alemeh Karami and Karl Refenner/BOKU Versuchszentrum for providing nut samples. The authors also thank the HSRM Project NANOBILD for infrastructure support, and are grateful for critical mathematical contributions by Mehmet Can Uçar (IST Austria) and discussions with Martin Niedermeier. The authors acknowledge funding from the European Research Council under the European Union's Horizon 2020 research and innovation programme (ERC grant 681885) and the Max Planck Society. Open access funding provided by University of Natural Resources and Life Sciences Vienna (BOKU).

Conflict of Interest

The authors declare no conflict of interest.

Author Contributions

This paper was conceptualized by N.G., S.J.A., J.C.H. Data acquisition and analysis being carried out by J.C.H., S.J.A., J.B., N.X.. Funding and resources were arranged by N.G., M.E., J.K. The original draft was prepared by J.C.H. All authors were involved in interpretation and review of the paper.

Keywords

3D imaging, pericarp, synzoochory, testa, tissue and shell mechanics

Received: July 2, 2020
Revised: September 3, 2020
Published online: October 20, 2020

[1] M. C. Stoddard, E. H. Yong, D. Akkaynak, C. Sheard, J. A. Tobias, L. Mahadevan, *Science* **2017**, *356*, 1249.
[2] S. H. Church, S. Donoughe, B. A. S. de Medeiros, C. G. Extavour, *Nature* **2019**, *571*, 58.
[3] O. J. Sexton, J. E. Bramble, I. L. Heisler, C. A. Phillips, D. L. Cox, *J. Chem. Ecol.* **2005**, *31*, 2391.
[4] E. N. Hahn, V. R. Sherman, A. Pissarenko, S. D. Rohrbach, D. J. Fernandes, M. A. Meyers, *J. R. Soc., Interface* **2017**, *14*, 20160804.
[5] A. Lazarus, H. C. B. Florijn, P. M. Reis, *Phys. Rev. Lett.* **2012**, *109*, 144301.
[6] V. Radchuk, L. Borisjuk, *Front. Plant Sci.* **2014**, *5*, 510.
[7] C. Dardick, A. M. Callahan, *Front. Plant Sci.* **2014**, *5*, 284.
[8] S. J. Antreich, N. Xiao, J. C. Huss, N. Horbelt, M. Eder, R. Weinkamer, N. Gierlinger, *Adv. Sci.* **2019**, *6*, 1900644.
[9] P. Schüler, T. Speck, A. Bührig-Polaczek, C. Fleck, *PLoS One* **2014**, *9*, e102913.
[10] S. B. Van der Wall, *Bot. Rev.* **2001**, *67*, 74.
[11] J. D. Bewley, *Plant Cell* **1997**, *9*, 1055.
[12] S. Sallon, E. Cherif, N. Chabrillange, E. Solowey, M. Gros-Balthazard, S. Ivorra, J. F. Terral, M. Egli, F. Aberlenc, *Sci. Adv.* **2020**, *6*, eaax0384.
[13] J. S. Jennings, N. H. Macmillan, *J. Mater. Sci.* **1986**, *21*, 1517.
[14] K. Sperber, T. Steinbrecher, K. Graeber, G. Scherer, S. Clausing, N. Wiegand, J. E. Hourston, R. Kurre, G. Leubner-Metzger, K. Mummenhoff, *Nat. Commun.* **2017**, *8*, 1868.
[15] R. L. Geneve, C. C. Baskin, J. M. Baskin, K. M. G. Gehan Jayasuriya, N. S. Gama-Arachchige, *Seed Sci. Res.* **2018**, *28*, 186.
[16] T. Steinbrecher, G. Leubner-Metzger, *Curr. Opin. Genet. Dev.* **2018**, *51*, 1.
[17] J. Nicolás-Bermúdez, I. Arzate-Vázquez, J. J. Chanona-Pérez, J. V. Méndez-Méndez, G. A. Rodríguez-Castro, H. Martínez-Gutiérrez, *Plant Physiol. Biochem.* **2018**, *132*, 566.
[18] A. Melelli, O. Arnould, J. Beaugrand, A. Bourmaud, *Molecules* **2020**, *25*, 632.
[19] A. V. Dyskin, Y. Estrin, A. J. Kanel-Belov, E. Pasternak, *Adv. Eng. Mater.* **2001**, *3*, 885.
[20] S. Krauss, E. Monsonego-Ornan, E. Zelzer, P. Fratzl, R. Shahar, *Adv. Mater.* **2009**, *21*, 407.
[21] C. Gao, B. P. J. Hasseldine, L. Li, J. C. Weaver, Y. Li, *Adv. Mater.* **2018**, *30*, 1800579.
[22] M. Mirkhalaf, T. Zhou, F. Barthelat, *Proc. Natl. Acad. Sci. USA* **2018**, *115*, 9128.
[23] J. M. Gómez, E. W. Schupp, P. Jordano, *Biol. Rev.* **2019**, *94*, 874.
[24] E. Munz, H. Rolletschek, S. Oeltze-Jafra, J. Fuchs, A. Guendel, T. Neuberger, S. Ortleb, P. M. Jakob, L. Borisjuk, *New Phytol.* **2017**, *216*, 1181.
[25] S. Penfield, *Curr. Biol.* **2017**, *27*, R853.
[26] J. Y. Juang, P. Y. Chen, D. C. Yang, S. P. Wu, A. Yen, H. I. Hsieh, *Sci. Rep.* **2017**, *7*, 14205.
[27] A. T. Moles, D. D. Ackerly, C. O. Webb, J. C. Twiddle, J. B. Dickie, M. Westoby, *Science* **2005**, *307*, 576.
[28] P. Gerrienne, B. Meyer-Berthaud, M. Fairon-Demaret, M. Street, P. Steemans, *Science* **2004**, *306*, 856.
[29] T. R. Paulsen, L. Colville, I. Kranner, M. I. Daws, G. Högstedt, V. Vandvik, K. Thompson, *New Phytol.* **2013**, *198*, 496.
[30] C. J. van der Kooi, J. Ollerton, *Science* **2020**, *368*, 1306.
[31] S. B. Vander Wall, *Philos. Trans. R. Soc., B* **2010**, *365*, 989.
[32] J. Igea, E. F. Miller, A. S. T. Papadopulos, A. J. Tanentzap, *PLoS Biol.* **2017**, *15*, e2002792.